New noncontact sensor for detecting pulmonary tumors during VATS

Koichi Akayama, MD[1], Yoshihiro Miyata, MD, PhD[2], Tomohiro Kawahara, PhD[3], Morihito Okada, MD, PhD[2], Makoto Kaneko, PhD[4], and Masazumi Okajima, MD, PhD[5] , Hideki Ohdan, MD, PhD[1]

[1]Department of Surgery, Division of Frontier Medical Science, and [2]Department of Surgical Oncology, Division of Genome Radiobiology and Medicine, Programs for Biomedical Research; Graduate School of Biomedical Sciences, Hiroshima University

[3] Frontier Research Academy for Young Researchers, Kyusyu Institute of Technology

[4] Department of Mechanical Engineering, Osaka University

[5] Department of Surgery, Hiroshima City Hiroshima Citizens Hospital

Corresponding author: Yoshihiro Miyata, MD, Ph.D.
Department of Surgical Oncology, Division of Genome Radiobiology and Medicine
Programs for Biomedical Research, Graduate School of Biomedical Sciences
Hiroshima University, 1-2-3 Kasumi, Minami-ku, Hiroshima 734-8551, Japan
Tel: +81-82-257-5222; Fax: +81-82-257-5224

E-mail: ymiyata@hiroshima-u.ac.jp

Sources of support: This work was partly supported by Grants-in-Aid for Scientific Research (KAKENHI) 18659405 and 19591627 from the Ministry of Education, Culture, Sports, Science and Technology (MEXT) of Japan, and the 21st Century COE Program "COE on Hyper Human Technology toward the 21st Century Industrial Revolution" from MEXT, Japan.

Author's contribution to the manuscript:
This study was conceived and designed by Yoshihiro Miyata, Tomohiro Kawahara, Makoto Kaneko and Masazumi Okajima. Koichi Akayama, Yoshihiro Miyata and Tomohiro Kawahara collected, analyzed and interpreted the data. Koichi Akayama, Yoshihiro Miyata wrote this manuscript. Morihito Okada, Makoto Kaneko, Masazumi Okajima and Hideki Ohdan provided critical revisions that are important for the intellectual content. The final version of the manuscript was approved by Yoshihiro Miyata and Hideki Ohdan.

Running title: Noncontact sensor for pulmonary nodules

Word count

Abstruct: 250 words

Mini-Abstract: 45 words

Text: 3,182 words

Abstract

Objective: Small pulmonary tumors are difficult to localize during video-assisted thoracic surgery (VATS) due to lack of direct tissue contact. However, in partial lung resection, tumor localization is quite important. The aim of this study was to evaluate the safety and feasibility of a new noncontact sensor for detecting pulmonary nodules during VATS using human and porcine models.

Methods: The sensor, based on the principle of phase differences, comprises an air nozzle for producing air pulse jets and optical fiber sensor to measure phase differences and visualize object stiffness. For *in vivo* assessment, we developed a porcine model by inserting plastic balls mimicking tumors into the pig lungs after thoracotomy and then scanned the lungs. The sensor sensitivity was evaluated by measuring the ratio of the depth of the ball from the lung surface to the ball diameter (D/S). For the *ex vivo* human model, partially resected lung tissue with tumors was obtained from six patients and then scanned.

Results: In the porcine model, 32 of 37 (86.5%), 70 of 94 (74.5%), and 60 of 100 (60.0%) tumors were detected in the categories D/S $\leqq$ 1, 1 < D/S $\leqq$ 2, and D/S > 2, respectively. Sensor safety was confirmed with an air jet of between 0.05 and 0.15 MPa directed onto the lung surface: all the examined lungs including the pleura remained

intact microscopically. In six patients, all nodules were successfully detected.

Conclusion: Our noncontact sensor is a safe and feasible tool for detecting small pulmonary tumors during VATS. (250 words)

Mini-Abstract: We designed a noncontact sensor based on the principle of phase differences for detecting small pulmonary tumors during video-assisted thoracic surgery. We confirmed the sensor's safety and feasibility as a diagnostic tool both *in vivo* and *ex vivo* by using porcine and human models, respectively. (45 words)

INTRODUCTION

With the improving performance of computed tomography (CT), the incidence of detection of small peripheral pulmonary nodules has increased (1,2). Recently, video-assisted thoracic surgery (VATS) has been proposed as a less-invasive approach for the resection of pulmonary tumors in selected patients (3,4). Although VATS has the advantage of being less invasive, a major problem associated with this method is the difficulty to intraoperatively localize pulmonary nodules by hand (5). Especially, detection is difficult after lung deflation by one-lung ventilation to ensure working space during the surgical procedure, because the nodule position changes from that determined by the CT scan; therefore, the CT data cannot be utilized during VATS. In anatomical segmentectomy or lobectomy, tumor localization is not mandatory. However, in the case of partial lung resection, which is the approach often chosen for an indeterminate nodule, localization of the nodule during surgery is quite important. Therefore, we developed a noncontact sensor for detecting pulmonary tumors during VATS. In this study, we also examined the safety and feasibility of the sensor by using human and porcine models.

MATERIALS AND METHODS

Principle of the sensor

Figure 1 shows the working principle of the noncontact sensor. Object displacement by air jet flow is measured on the basis of the relationship between the reflected light quantity and distance from the tissue surface (Fig. 1a). The distance sensor provides sinusoidal output with individual phases for the air pulse jets (Fig. 1b). When the sensor scans a tumor, the output from the optical fiber sensor changes due to the presence of the tumor (Fig. 1c). The phase difference between the input force and output of the distance sensor is displayed directly on a monitor in real time.

By plotting the input force and output distance onto the horizontal and vertical axes of an oscillograph to draw a Lissajous diagram, one can clearly detect a change in phase α, which in turn reflects an increase in stiffness, such as that caused by a tumor in lung tissue (Fig. 2a,b). As shown in Figure 2c, the plastic ball could be detected by the sensor based on the change in the Lissajous patterns after 4.7 seconds of scanning.

Figure 3 shows the noncontact sensor, comprising an air nozzle, an optical fiber-based distance sensor (FU-4F; Keyence, Tokyo, Japan), and a pressure sensor (AP-43; Keyence) to measure the input force. The total diameter of the sensor tip is 10 mm,

which is sufficiently small for application during the surgical procedure.

Sensor measurement system

Figure 4 shows the measurement system of the noncontact sensor. The system is composed of three parts: (1) air supply system with an air compressor and solenoid valves for providing the air pulse jets, (2) sensor head, and (3) personal computer (PC) for controlling the air pressure and obtaining data from both the pressure sensor and optical fiber sensor. The PC sends a periodic on–off signal to the solenoid valve and outputs from the sensors are fed into the PC through an analog-to-digital (AD) converter.

Porcine model experiment

To examine the safety and feasibility of the sensor *in vivo*, we developed a porcine model using six male castrated pigs (12 weeks old, 40 kg). Medetomidine and midazolam (40 μg/kg each) were mixed and intramuscularly injected into the pigs. Then, 10 μg/kg of pentobarbital was injected intravenously. Univent tubes were intubated to produce one-lung ventilation. Under general anesthesia (2–3% isoflurane inhalation), the pigs were mechanically ventilated and thoracotomy was performed. All animals

have received humane care in compliance with the Guide for the Care and Use of Laboratory Animals (www.nap.edu/catalog/5140.html). This experiment was conducted in accordance with the guidelines for the care of animal subjects, as defined by the Institutional Review Board of Olympus Corporation (Hachioji, Japan).

***Determination of the sensor setting* in vivo**

To determine the *in vivo* sensor setting, we first tested the sensor performance by changing the distance between the nozzle and optical fiber sensor (4–8 mm), frequency of the pulse input (20–60 Hz), and pressure of the input (0.08–0.15 MPa). We also tested whether the operation theater lighting and animal heartbeats affect the results.

Detection performance of the sensor

Plastic balls mimicking tumors were randomly inserted in the deflated lung from the back-side surface, and the lung was then scanned with the sensor from a contralateral normal pleura side. This method did not induce distortion of both the lung pleural surface and lung parenchyma to be scanned with the sensor.

After the measurement, the lung was inflated to restore its normal volume. Depth from the lung surface (D) was measured by using a small needle pierced from the lung

surface to the plastic ball. By changing the depth (1–24 mm) and the ball diameter (S; 5–10 mm), we evaluated the sensitivity of this method on the basis of the D/S ratio. The measurements were performed 10 times for each setting. A phase difference exceeding the threshold value (30°) on more than 7 of 10 measurements was defined as a positive detection. We determined the appropriate input frequency and pressure to be 40 Hz and 0.08 MPa, respectively.

Sensor safety

To examine the safety of the sensor, we directed periodic air jets onto the lung surface at pressures between 0.05 and 0.15 MPa for up to 30 s. Then, we partially resected the tested lung tissue and fixed it with 10% formalin for pathologic examination.

Human model experiment

Six lung lobes containing tumors were removed surgically and scanned *ex vivo* with the sensor. Pathologic diagnosis, tumor size (S), and depth from the lung surface (D) were measured by a preoperative CT scan, and the D/S ratios were calculated. We obtained appropriate approval for the study from the Institutional Review Board of Hiroshima University, which waived the requirement for informed consent from the individual

patients.

Statistical analysis

Receiver-operating characteristic (ROC) curve analysis for the prediction of positive detection of the plastic ball was performed to determine the optimal cutoff *D*/*S* ratio. Data were statistically analyzed by using EZR (Saitama Medical Centre, Jichi Medical University, Kanda, Japan, 2012), which is a graphic user interface for R version 2.13.0 (The R Foundation for Statistical Computing, Vienna, Austria).

RESULTS

Determination of the sensor setting *in vivo*

Based on the preliminary experiment that used an experimental model consisting of silicone rubber with a small plastic ball embedded inside to mimic lung tissue and a lung nodule, we decided to set the sensor input at a frequency of around 40 Hz and a pressure of around 0.08 MPa(6). We confirmed that this setting was not affected when live animal lung with the heart beating was used. Further, the operation theatre lighting and animal heartbeats also did not influence the sensor performance.

Sensor sensitivity

We measured the lungs of the same animals before the insertion of the balls in six animals in which no tumors were detected (0/6).

Figure 5a shows the experimental results in the porcine model. By measuring the D/S ratios, 32 of 37 (86.5%), 70 of 94 (74.5%), and 60 of 100 (60.0%) tumors were detected in the categories $D/S \leqq 1$, $1 < D/S \leqq 2$, and $D/S > 2$, respectively.

Figure 5b shows the ROC curves of the *D*/*S* ratio. The area under the curve was 0.620 (95% confidence interval [CI]: 0.542–0.697) at a cutoff of 2.2, with a specificity of 0.630 and sensitivity of 0.580.

Sensor safety

Figure 6 shows the microscopic findings on hematoxylin–eosin staining after an air jet of 0.15 MPa at 30 Hz was directed onto the lung surface for 30 s. Lung structures including the pleura and alveoli were not destroyed even under the most traumatic conditions.

Human model experiment

Table 1 shows the patients characteristics in the human model. The diameter of the nodules ranged from 5.9 mm to 21.5 mm and the depth from the lung surface ranged from 0.16 mm to 34.0 mm, as measured by the preoperative CT scan. Consequently, the D/S ratio ranged from 0.01 to 3.27. In five patients, all the nodules including those categorized as D/S >2 were successfully identified.

Figure 7a shows the CT finding in patient 6. The tumor was located at a 34-mm depth from the lung surface and was 15 mm in diameter. The tumor was identified by the sensor during the surgical procedure (Fig. 7b).

DISCUSSION

Various methods to detect small pulmonary tumors during VATS have been reported, and are roughly divided into two groups: preoperative CT-guided marking and intraoperative localization of the pulmonary nodule. The preoperative method includes tumor marking by using hook wire, coil, dye, technetium, contrast medium, or lipiodol (7-15). These materials are injected into the lung surface close to the pulmonary nodule and localization is carried out through a fluoroscope or detector during the operation. However, these methods can cause serious complications such as pneumothorax, hemorrhage, and fatal air embolism (16,17). Intraoperative localization techniques such

as ultrasonography (18,19) and contact sensor use (20,21) have been reported.

In this study, we have developed a new device that uses an air jet flow instead of direct tissue contact by the sensor tip. The stiffness of the tissue is visualized by measuring the tissue displacement with the optical fiber sensor. Our sensor offers a number of advantages over the conventional intraoperative localization techniques. Because the sensor does not directly contact the tissue to be inspected, tissue damage is avoided. Noncontact sensing may also increase the speed and efficiency of the scan, whereas a contact sensor can inspect only a small area of the lung. On average, it takes approximately 3 minutes to scan an entire lung by using our device. Complete collapse of the lung is not mandatory for tumor detection using our sensor, whereas small amounts of residual air in the lung usually prevent adequate examination by ultrasonography. By applying the optical fiber sensor as a displacement sensor, we reduced the device size to allow insertion into the chest cavity via a small hole. The disadvantage of using an optical fiber sensor is that the output can be influenced by the color as well as the inclination angle of the tissue. To resolve this problem, we focused on the phase difference (6).

In our experimental model, we decided on using a phase difference exceeding the threshold value (30°) of more than 7 of 10 measurements as a positive detection.

However, in some case**s,** especially if the ball was near the lung surface, we could guess the existence of the ball by visually observing the deformity of the lung surface made by airflow. The human eye must be the excellent detector in such a case. For clinical application, we can combine a phase difference measured by the optical fiber sensor and a visual finding of the lung surface produced by the airflow to detect the existence of the tumor.

Suzuki et al. (22) have indicated that if the distance to the pleural surface is more than 5 mm for nodules of less than10 mm in size, the probability of detection failure is 63%. Saito et al. (23) reported the relationship between the diameter and distance from the lung surface of a pulmonary nodule. From the reports, the detection limit of tumors in VATS and open thoracotomy is a D/S ratio of less than around 1 and 2, respectively. In our porcine model experiment, almost 90% of the nodules smaller than 10 mm were detected with a D/S ratio of less than 1. Generally, normal porcine lungs are much harder and smaller than human lungs. Consequently, detection of the nodules by utilizing the difference in stiffness between the nodules and surrounding normal tissue in a porcine model is more difficult than in human lungs. In fact, in human lungs resected in our study, all nodules including those with a D/S ratio of more than 2 were successfully identified by the sensor. As this noncontact sensor is sensitive enough to

detect small pulmonary nodules during VATS, it may possible to completely avoid preoperative marking.

One may be concerned whether the sensor can distinguish pulmonary tumors from normal lung structures such as bronchi and vessels. During the scan process, we found that normal bronchi and vessels resembled a tree. If a nodule is detected by the sensor in peripheral lung tissue such as the bronchi, it is easy to differentiate the bronchi by scanning the circumference of the solitary nodule. If the tumor exists deeper from the lung surface and is adjacent to the proximal bronchi and vessels, it may difficult to detect the tumor by using our sensor. However, in such cases, anatomical segmentectomy or lobectomy is usually performed for tumor removal. Tumor localization with our sensor is necessary only during VATS for partial resection of the tumor.

In this study, we found that normal lung tissue was very soft and easy to deform by using a small amount of air pressure, suggesting relative ease in exposing a nodule. Our results clearly demonstrate that our non-contact sensor can provide reproducible measurements of lung consistency. The limitations of this study include the fact that the porcine model differed from the actual condition observed in clinical settings. In clinical application, diagnostic performance might differ between patients with emphysematous

patterns and those with fibrotic patterns . In the porcine model, the lung is normal . In addition, the stiffness of the tumor has wide variations clinically, such as localized bronchioloalveolar carcinoma and adenomatous hyperplasia. We are now conducting a clinical trial to apply our device in patients undergoing tumor resection via VATS.

In conclusion, we believe that our noncontact sensor is a safe and feasible tool for identifying small pulmonary tumors during VATS.

REFERENCES

1. Kaneko M, Eguchi K, Ohmatsu H, et al. Peripheral lung cancer: screening and detection with low-dose spiral CT versus radiography. *Radiology* 1996; 201:798-802.
2. Remy-Jardin M, Remy J, Giraud F, et al. Pulmonary nodules: detection with thick-section spiral CT vs. conventional CT. *Radiology* 1993; 187:513-520.
3. Mack MJ, Aronnoff RJ, Acuff TE, et al. Present role of the chest. *Ann Thorac Surg* 1992; 54:403-409.
4. Landreneau RJ, Hazelrigg SR, Ferson PF, et al. Thoracoscopic resection of 85 pulmonary lesions. *Ann Thorac Surg* 1992; 54:415-420.
5. Gagliano RA, Reinschmidt JP, Murray SP, et al. A novel method of transthoracic lung nodule localization. *Curr Surg* 1999; 56:410-412.
6. Kawahara T, Toya C, Tanaka N, et al. Non-contact impedance imager with phase differentiator. *IEEE BioRob* 2006; 159:1-6.
7. Shepard JO, Mathisen DJ, Muse VV, et al. Needle localization of peripheral lung nodules for video-assisted thoracoscopic surgery. *Chest* 1994; 105:1559-1563.
8. Mack MJ, Goldon MJ, Postma TW, et al. Percutaneous localization of pulmonary nodules for thoracoscopic lung resection. *Ann Thorac Surg* 1992; 53:1123-1124.

9. Asamura H, Kondo H, Naruke T, et al. Computed tomography-guided coil injection and thoracoscopic pulmonary resection under roentgenographic fluoroscopy. *Ann Thorac Surg* 1994; 58:1542-1544.

10. Jangra D, Powell T, Kalloger SE, et al. CT-directed microcoil localization of small peripheral lung nodules: a feasibility study in pigs. *J Invest Surg* 2005 Sep; 18:265-272.

11. Nomori H, Horio H. Colored collagen is a long-lasting point marker for small pulmonary nodules in thoracoscopic operation. *Ann Thorac Surg* 1996; 61:1070-1073.

12. Wicky S, Mayor B, Cuttat JF, et al. CT-guided localizations of pulmonary nodules with methylene blue injections for thoracoscopic resections. *Chest* 1994; 106:1326-1328.

13. Chella A, Lucchi M, Ambrogi MC, et al. A pilot study of the role of TC-99 radionuclide in localization of pulmonary nodular lesions for thoracoscopic resection. *Eur J Cardiothorac Surg* 2000; 18:17-21.

14. Moon SW, Wang YP, Jo KH, et al. Fluoroscopy-aided thoracoscopic resection of pulmonary nodule localized with contrast media. *Ann Thorac Surg* 1999; 68:1815-1820.

15. Watanabe K, Nomori H, Ohtsuka T, et al. Usefulness and complications of computed tomography-guided lipiodol marking for fluoroscopy-assisted thoracoscopic resection of small pulmonary nodules: experience with 174 nodules. *J Thorac Cardiovasc Surg* 2006; 132:320-324.al

16. Horan TA, Pinheiro PM, Araujo LM, et al. Massive gas embolism during pulmonary nodule hook wire localization. *Ann Thorac Surg* 2002; 73:1674-1649.

17. Sakiyama S, Kondo K, Matsuoka H, et al. Fatal air embolism during computed tomography-guided pulmonary marking with a hook-type marker. *J Thorac Cardiovasc Surg* 2003; 126:1207-1209.

18. Santambrogio R, Montorsi M, Bianchi P, et al. Intraoperative ultrasound during thoracoscopic procedures for solitary pulmonary nodules. *Ann Thorac Surg* 1999; 68:218-222.

19. Mattioli S, D'Ovidio F, Daddi N, et al. Transthoracic endosonography for intraoperative localization of lung nodules. *Ann Thorac Surg* 2005; 79:443-449.

20. Otsuka T, Furuse A, Kohno T, et al. Application of a new tactile sensor to thoracoscopic surgery: experimental and clinical study. *Ann Thorac Surg* 1995; 60:610-614.

21. Weiss RE, Hartanto V, Perrotti M, et al. In vitro trial of the pilot prototype of the

prostate mechanical imaging system. *Urology* 2001; 58:1059-1063.

22. Suzuki K, Nagai K, Yoshida J, et al. Video-assisted thoracoscopic surgery for small indeterminate pulmonary nodules. *Chest* 1999; 115:563-568.

23. Saito H, Minamiya Y, Matsuzaki I, et al. Indication for preoperative localization of small peripheral pulmonary nodules in thoracoscopic surgery. *J Thorac Cardiovasc Surg* 2002; 124:1198-1202.

FIGURE LEGENDS

Figure 1

Working principal of the noncontact sensor based on phase difference. The sensor consists of an air nozzle producing air pulse jets to induce deformity and an optical fiber sensor to measure phase differences and visualize object stiffness. (a) Distance between the sensor and object is measured by the optical fiber sensor. (b) The distance sensors provide a sinusoidal output for the air pulse jets. (c) When the sensor scans a tumor, the output from the optical fiber sensor changes due to the presence of the tumor.

Figure 2

(a) A Lissajous diagram drawn by plotting the input force and the output displacement onto the horizontal and vertical axes of an oscillograph. (b) If a tumor is present in the tissue, phase α, indicated by a Lissajous diagram, would show a change. (C) Scanning result by the sensor. The tumor is detected based on the change in the Lissajous patterns.

Figure 3

The noncontact sensor with a sensor tip of 10-mm total diameter, consisting of an air nozzle and optical fiber sensor.

Figure 4

Measurement system of the noncontact sensor, comprising an air supply system for

providing air pulse jets, a sensor head, and a personal computer (PC).

Figure 5a

Sensitivity of the noncontact sensor in the porcine model, measured by the ratio of the depth of the ball from the lung surface to the ball diameter (D/S). The circles indicate successful detection whereas the crosses indicate detection failure.

Figure 5b

The *D*/*S* ratios derived from the area under the receiver-operating characteristic curve were used to predict positive detection. The optimal cutoff value was 2.2, with a specificity of 0.630 and a sensitivity of 0.580.

Figure 6

Hematoxylin–eosin staining of the lung tissue in the porcine model. (a), (c) Normal lung tissue without an air jet shot. (b), (d) Lung tissue after an air jet shot of 0.15 MPa at 30 Hz for 30 s. (a), (b): 40× magnification; (c), (d): 400× magnification.

Figure 7

Scan result of the noncontact sensor. (a) Computed tomography (CT) image of case 6. (b) Scan by the noncontact sensor during video-assisted thoracic surgery (VATS).

(3,182 words)

Table.1

case	age	sex	pathology	Size on CT (mm)	Depth on CT (mm)	Depth/ Size
1	75	M	**sq**	5.9	19.1	3.27
2	71	M	**ad**	18.7	0.16	0.01
3	65	F	**ad**	13.5	27.1	2.01
4	63	M	**ad**	10.3	11.0	1.03
5	71	F	**met**	21.5	21.5	1.00
6	72	M	**ad**	15.0	34.0	2.3

Sq: squamous cell carcinoma, Ad: adenocarcinoma, Met: Metastatic osteosarcoma

Figure.1

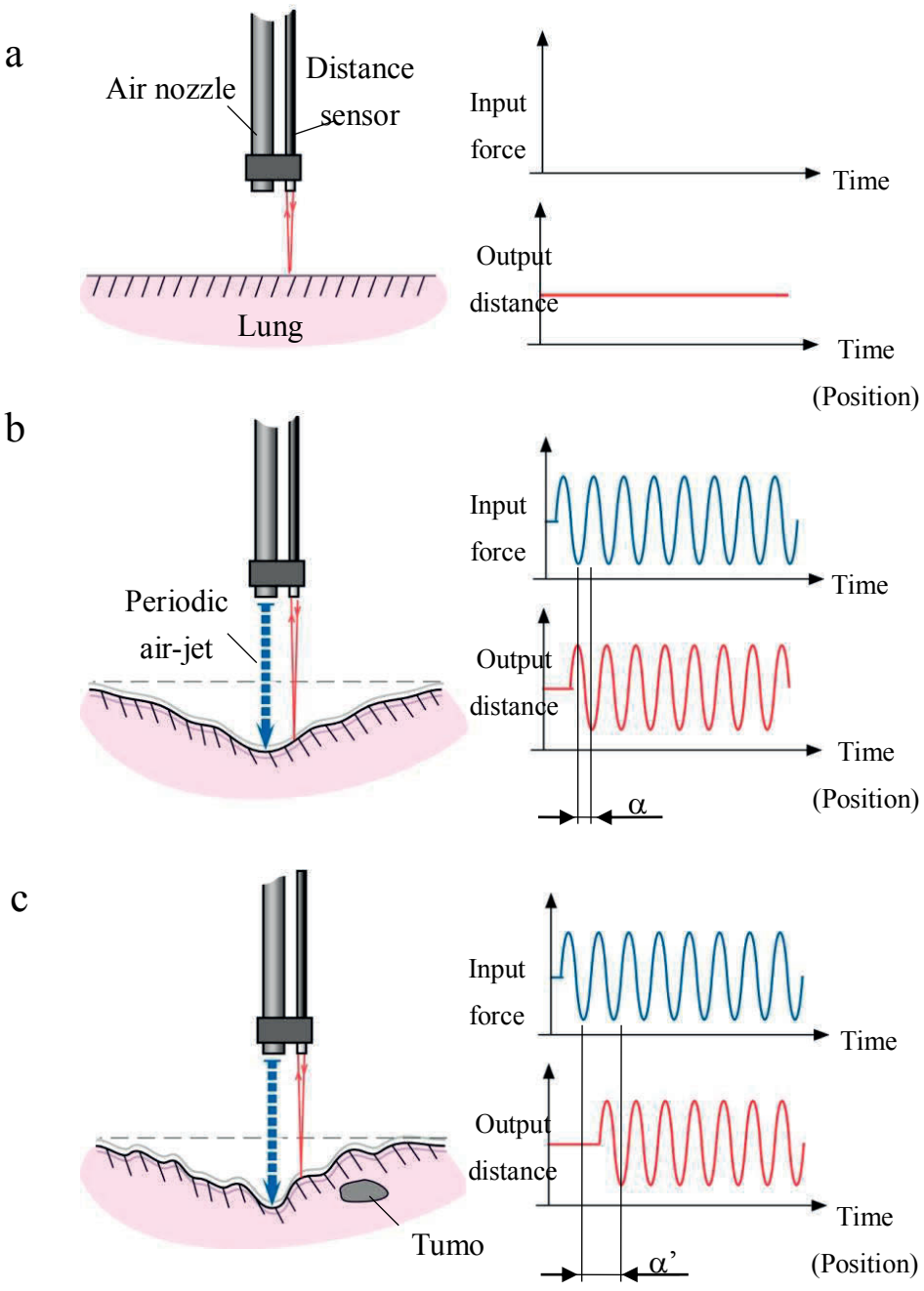
a
Air nozzle
Distance sensor
Lung
Input force
Time
Output distance
Time
(Position)
b
Periodic air-jet
Input force
Time
Output distance
Time
(Position)
α
c
Tumo
Input force
Time
Output distance
Time
(Position)
α'

Figure.2

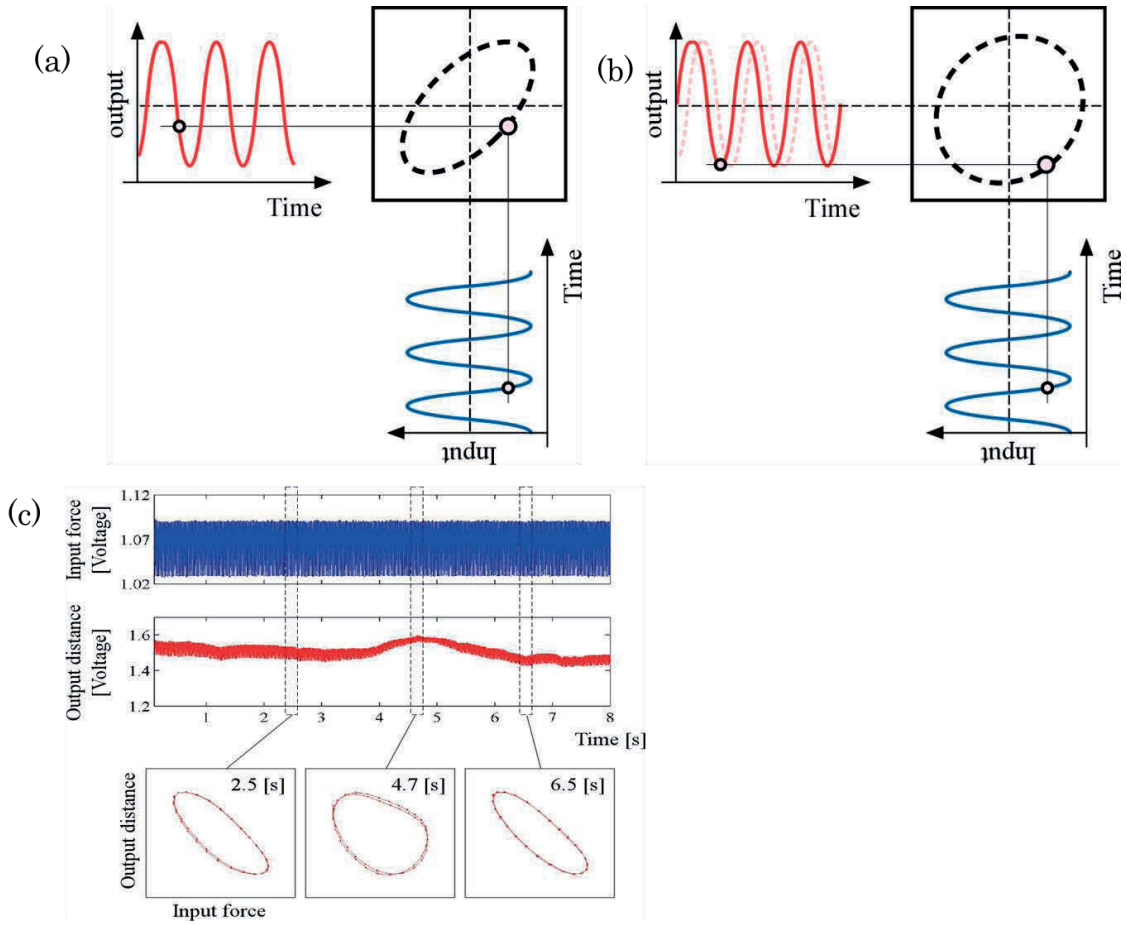
(a)
output
Time
Time
Input
(b)
output
Time
Time
Input
(c)
Input force [Voltage]
1.12
1.07
1.02
Output distance [Voltage]
1.6
1.4
1.2
1
2
3
4
5
6
7
8
Time [s]
Output distance
2.5 [s]
4.7 [s]
6.5 [s]
Input force

Figure.3

Figure.4

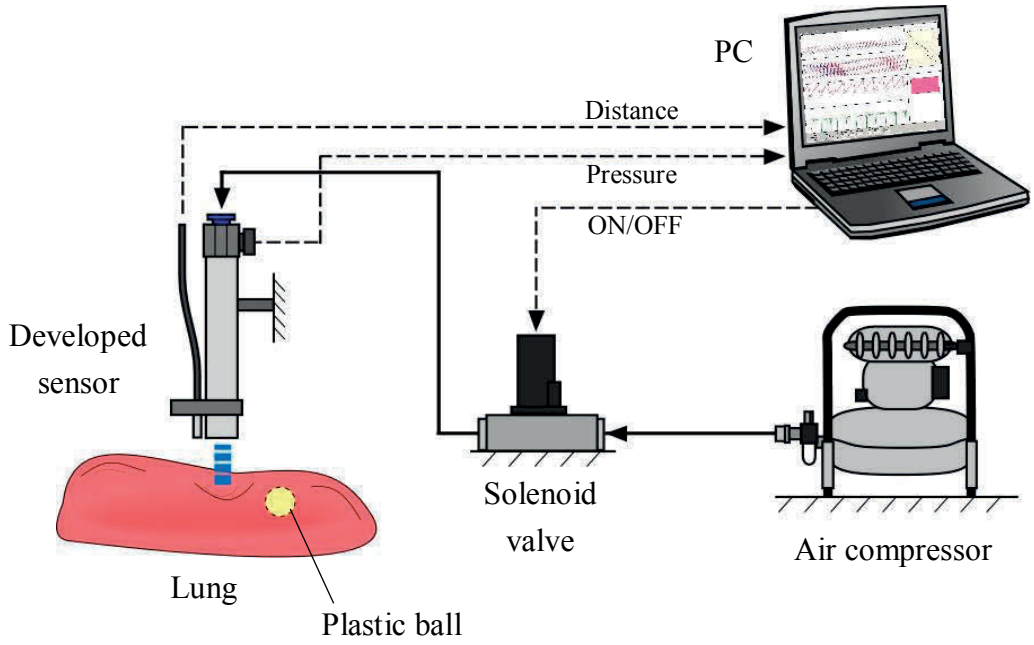
PC
Distance
Pressure
ON/OFF
Developed
sensor
Solenoid
valve
Air compressor
Lung
Plastic ball

Figure.5a

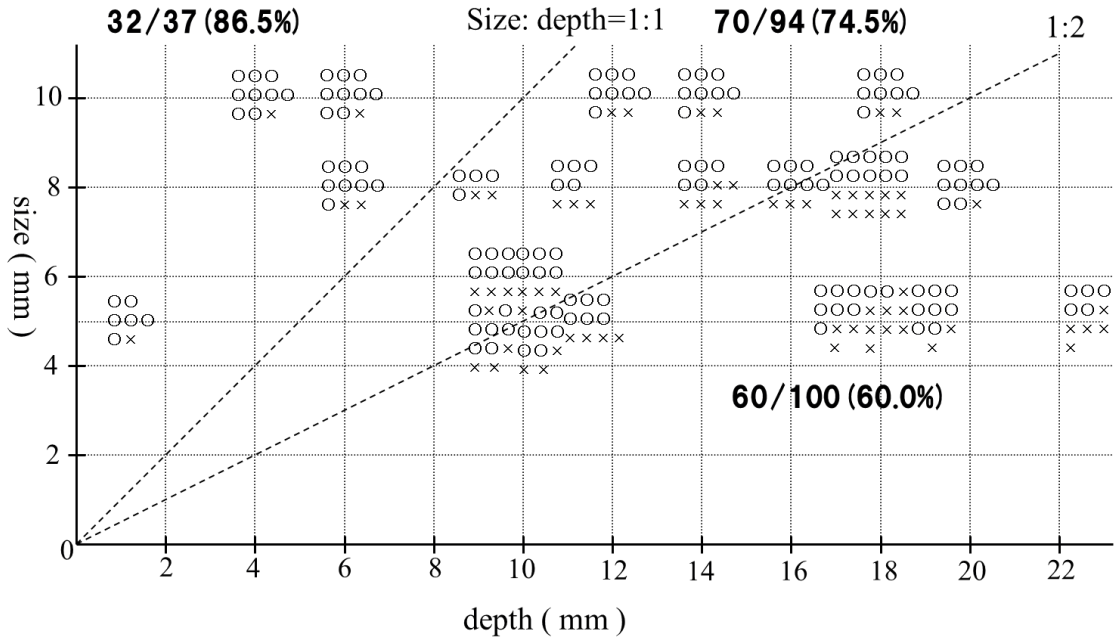
32/37 (86.5%)
Size: depth=1:1
70/94 (74.5%)
1:2
60/100 (60.0%)
size (mm)
depth (mm)
0
2
4
6
8
10
12
14
16
18
20
22

Figure.5b

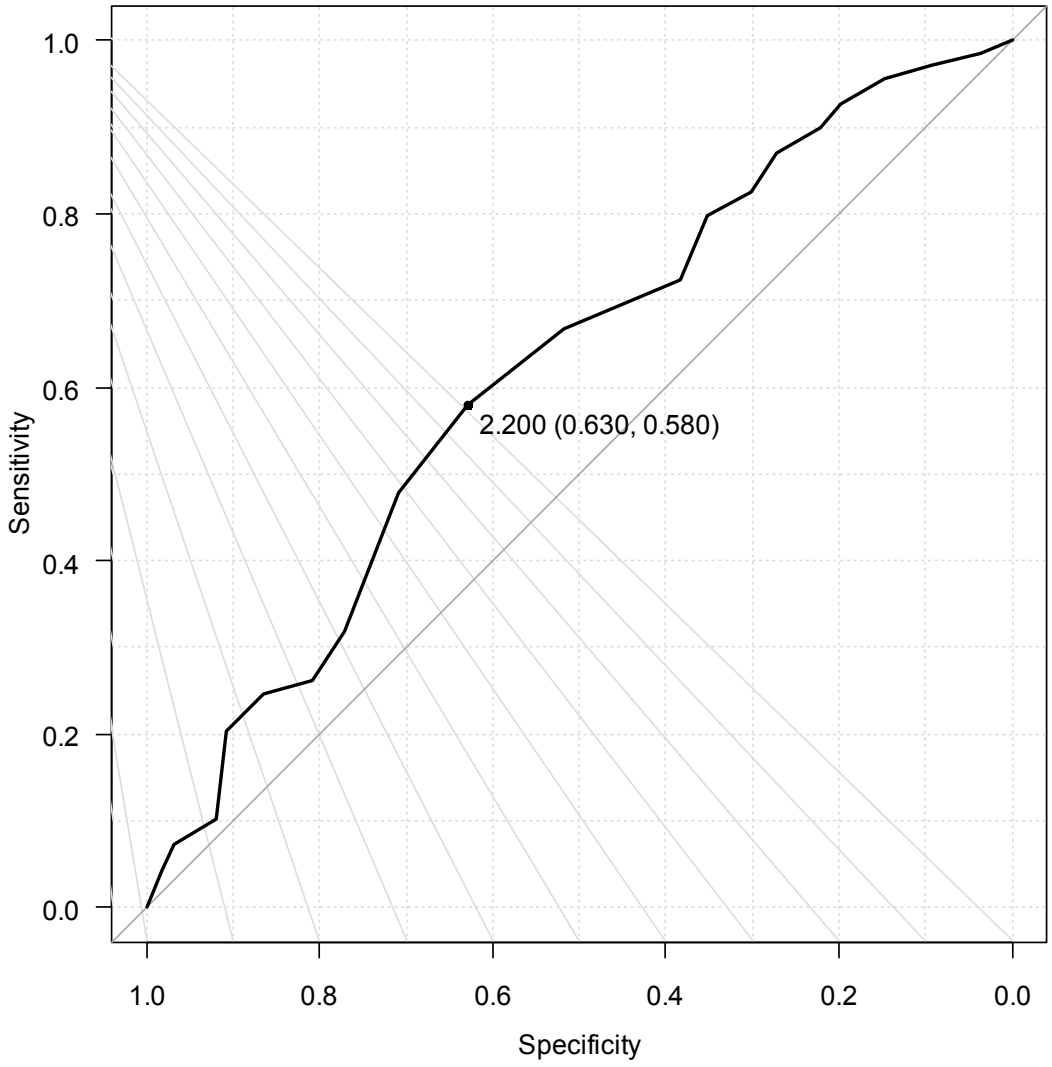
1.0
0.8
0.6
0.4
0.2
0.0
Sensitivity
2.200 (0.630, 0.580)
1.0
0.8
0.6
0.4
0.2
0.0
Specificity

Figure.6

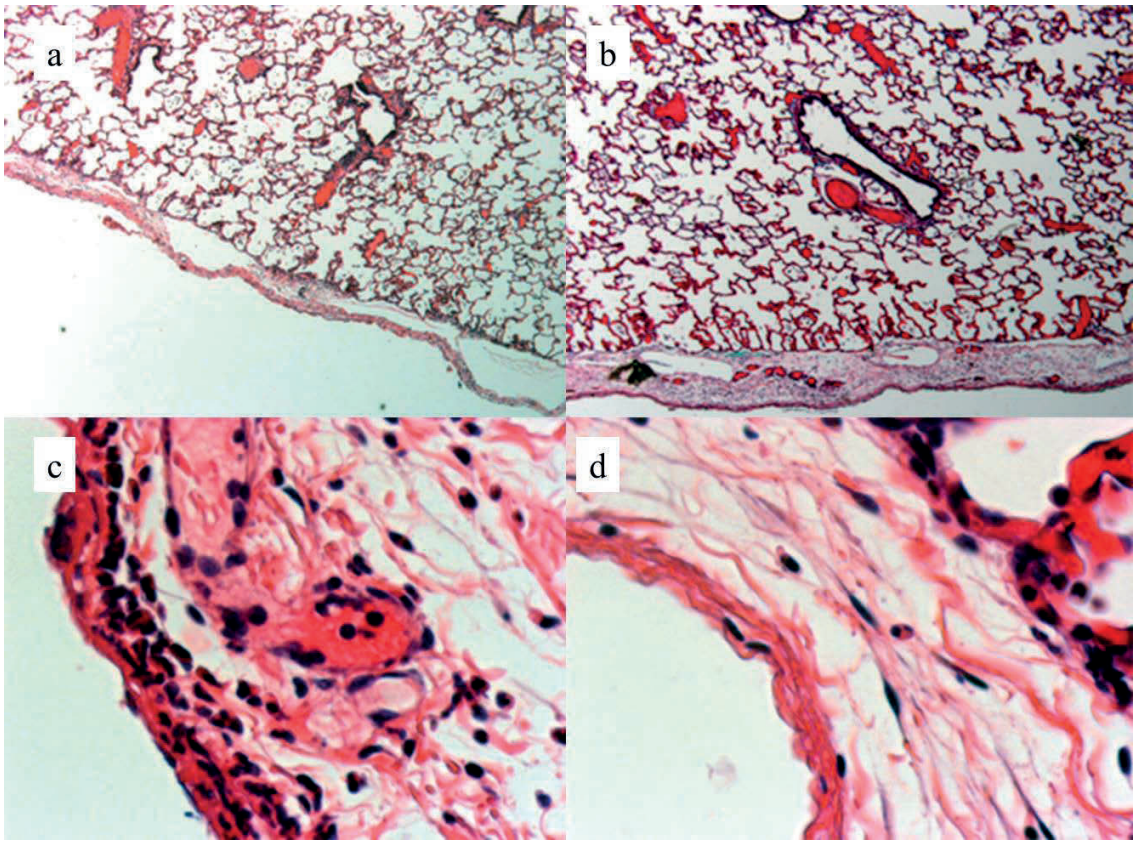

Figure.7